Volume 18 | Number 24 | 21 December 2018 | Pages 3707–3950

Lab on a Chip

Devices and applications at the micro- and nanoscale

rsc.li/loc

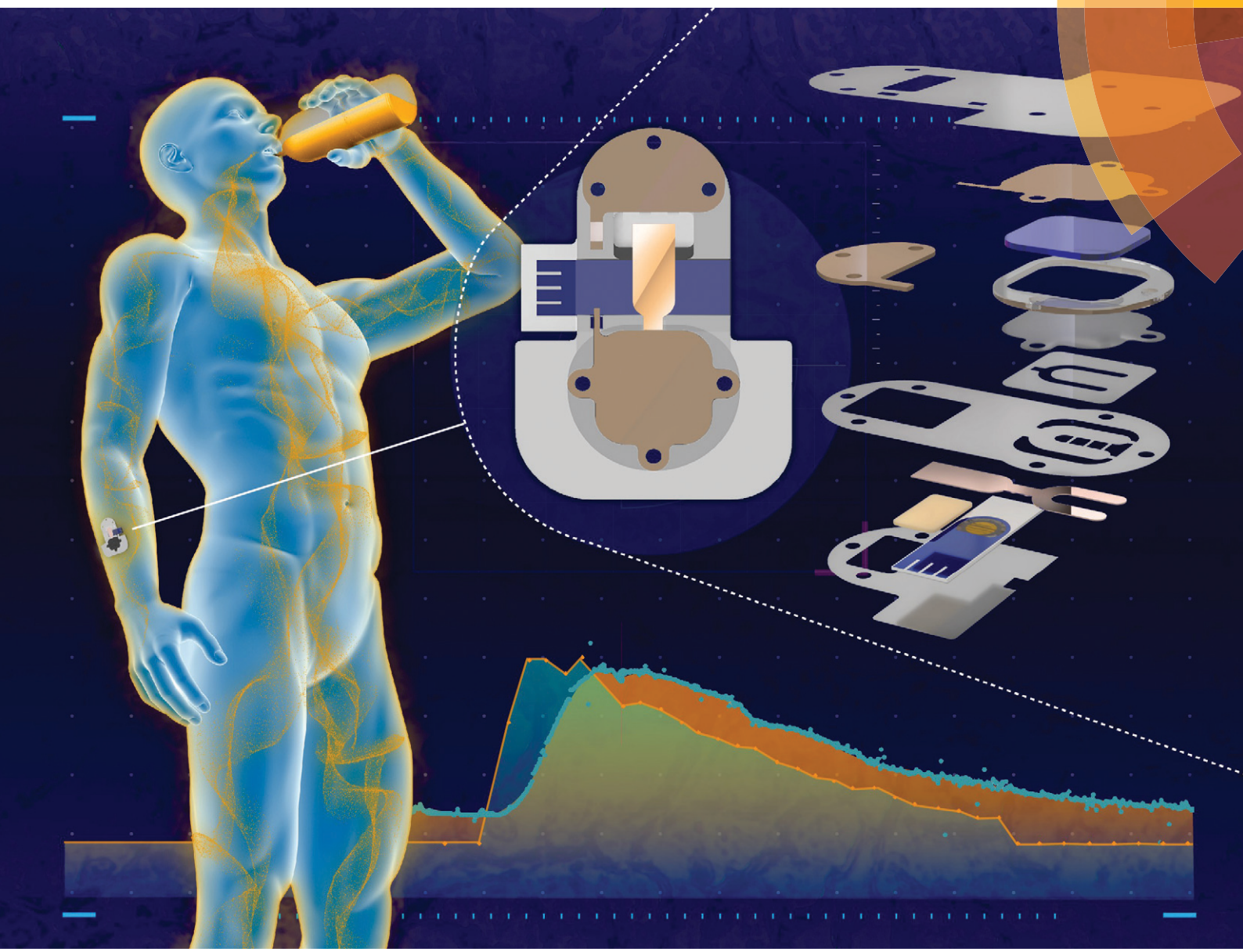

ISSN 1473-0197

ROYAL SOCIETY OF CHEMISTRY

PAPER

J. Heikenfeld *et al.*

Complete validation of a continuous and blood-correlated sweat biosensing device with integrated sweat stimulation

Lab on a Chip

PAPER

View Article Online
View Journal | View Issue

Cite this: *Lab Chip*, 2018, **18**, 3750

Complete validation of a continuous and blood-correlated sweat biosensing device with integrated sweat stimulation†

A. Hauke, [a] P. Simmers, [a] Y. R. Ojha,[b] B. D. Cameron,[b] R. Ballweg,[c] T. Zhang,[c] N. Twine, [a] M. Brothers,[d] E. Gomez [a] and J. Heikenfeld*[a]

Received 10th October 2018,
Accepted 1st November 2018

DOI: 10.1039/c8lc01082j

rsc.li/loc

A wearable sweat biosensing device is demonstrated that stimulates sweat and continuously measures sweat ethanol concentrations at 25 s intervals, which is then correlated with blood ethanol during a >3 hour testing phase. The testing involves a baseline condition (no ethanol) followed by a rapid blood and sweat rise of ethanol (oral bolus), and finally, the physiological response of the body as ethanol concentrations return to baseline (metabolized). Data sets include multiple *in vivo* validation trials and careful *in vitro* characterization of the electrochemical enzymatic ethanol sensor against likely interferents. Furthermore, the data is analyzed through known pharmacokinetic models with a strong linear Pearson correlation of 0.9474–0.9996. The continuous nature of the data also allows analysis of blood-to-sweat lag times that range between 2.3 to 11.41 min for ethanol signal onset and 19.32 to 34.44 min for the overall pharmacokinetic curve lag time. This work represents a significant advance that builds upon a continuum of previous work. However, unresolved questions include operation for 24 hours or greater and with analytes beyond those commonly explored for sweat (electrolytes and metabolites). Regardless, this work validates that sweat biosensing can provide continuous and blood-correlated data in an integrated wearable device.

Introduction

Eccrine sweat biosensing has seen a ~10× increase in academic publishing over the past 5 years, adding significant momentum to the advancement of wearable biosensing technology.[1] Along with interstitial fluid, saliva, and tears, sweat is a candidate biofluid for the emerging '3rd wave' of biosensing which promises continuous analyte access and measurement in a minimally- or non-invasive format.[2] For sweat, major progress has been required in both understanding the raw possibilities of the biofluid itself,[2] and in creating wearable technology to reliably access and sense analytes in sweat.[1,3–13] Despite all this progress, a significant milestone has not yet been achieved: validation of a continuous and blood-correlated sweat biosensing device. Previous device demonstrations (see ESI† Table S1), including those by our own research group, do not satisfy a complete set of requirements: (1) the sweat analyte must have potential for blood-correlation[2] which excludes sweat analytes such as Na^+ and lactate;[14] (2) for most analytes, sweat generation rate must be steady or measured due to the effects of analyte dilution[2,13] or sensor-dependencies on sweat rate;[15] (3) the ultra-small volumes of sweat must be quickly transported and coupled to sensors while minimizing analyte exchange with the skin or the transport materials themselves;[16] (4) for final validation, continuous raw data needs to be shown for the analyte in both sweat and blood to assure that numerous other confounding factors have been resolved (*e.g.*, influence of changing pH or salinity, sensor reversibility, body motion artifacts, *etc.*). Some of these requirements have been previously addressed in stand-alone demonstrations (see ESI† Table S1), but a continuous and blood-correlated sweat biosensing device remains to be demonstrated.

We report here complete validation of a continuous and blood-correlated sweat biosensing device with integrated sweat stimulation. This work unequivocally demonstrates that sweat can indeed be used to track blood level information with accuracy and relevant temporal resolution. Our chosen demonstration analyte is ethanol, a strong validation analyte because it is 1 : 1 between sweat and blood due to its small lipophilic nature.[2,13,17,18] Ethanol allows continuous measurement for >3 hours of a baseline condition followed by a rapid blood and sweat rise, and finally the physiological

[a] *Novel Devices Laboratory, College of Engineering, University of Cincinnati, Cincinnati, Ohio 45221, USA*
[b] *Biomedical Optics and Sensing Laboratory, Department of Bioengineering, University of Toledo, Toledo, Ohio 43606, USA*
[c] *College of Medicine, University of Cincinnati, Cincinnati, Ohio 45221, USA*
[d] *UES, Inc., Dayton, Ohio 45432, USA*

† Electronic supplementary information (ESI) available: AutoCAD device layout, sweat sensor assembly time-lapse, Tables S1–S6, and text + Fig. S1–S6. See DOI: 10.1039/c8lc01082j

response of the body as it metabolizes and decreases the ethanol concentrations back to baseline. Data sets include multiple *in vivo* validation trials, and careful *in vitro* characterization of the sensor against likely interferents. Furthermore, we are able to analyze both blood and sweat data through known pharmacokinetic models with a strong linear Pearson correlation of 0.9474–0.9996, which like for continuous glucose monitoring is an additional *in silico* capability that increases the predictive value of continuous wearable biochemical data.[2] The continuous nature of the data also allows us to characterize and discuss lag times that range between 2.3 to 11.41 min for ethanol signal onset and 19.32 to 34.44 min for the overall pharmacokinetic curve lag time. These important validation points are enabled by the completeness of the device and experimental design used here, and are beyond even what would be possible by combining features of previous sweat biosensing demonstrations (ethanol, glucose, methylxanthine).[19–24] The demonstration device is also highly reproducible as we provide detailed CAD drawings, bill of materials, time-lapse video of complete patch build-out, and experimental methods.

Although this work does represent a significant advance that builds upon a continuum of work by our group and others,[3–12,15,16] unresolved questions remain. Such questions include demonstration of such a device for 24 hours or greater and with analytes that represent a greater breakthrough than those already commonly explored for sweat (electrolytes and metabolites). Regardless, the work here sets the stage for others to begin this next phase of research which will be required before sweat biosensing can definitively prove its value in the emerging '3rd wave' of biosensing technology.[2]

Novel design and operation features

Fig. 1a provides size-accurate three-dimensional drawings of every material utilized in the system assembly.[25] The planar design allows assembly by stacking layers on an alignment tool (see Fig. 1a holes/dotted-lines, and ESI† Video S1) and uses a low-cost and scalable cut/laminate manufacturing paradigm. Nearly all of the materials are commercially available adhesives and films which are simply laser cut to size (see Methods section). Although electronics integration is not performed here, it has been previously demonstrated for sweat[3,8] and is a commercially mature technology even in a fully flexible format. Fig. 1b and c shows top and bottom views of fully assembled devices. Electronic instrumentation and interface connections are detailed in the Methods section and listed in the ESI† Table S2. Device operation is shown diagrammatically and described in Fig. 2. We will next discuss several design and operation features of the device that are novel with respect to publications by research groups other than our own.

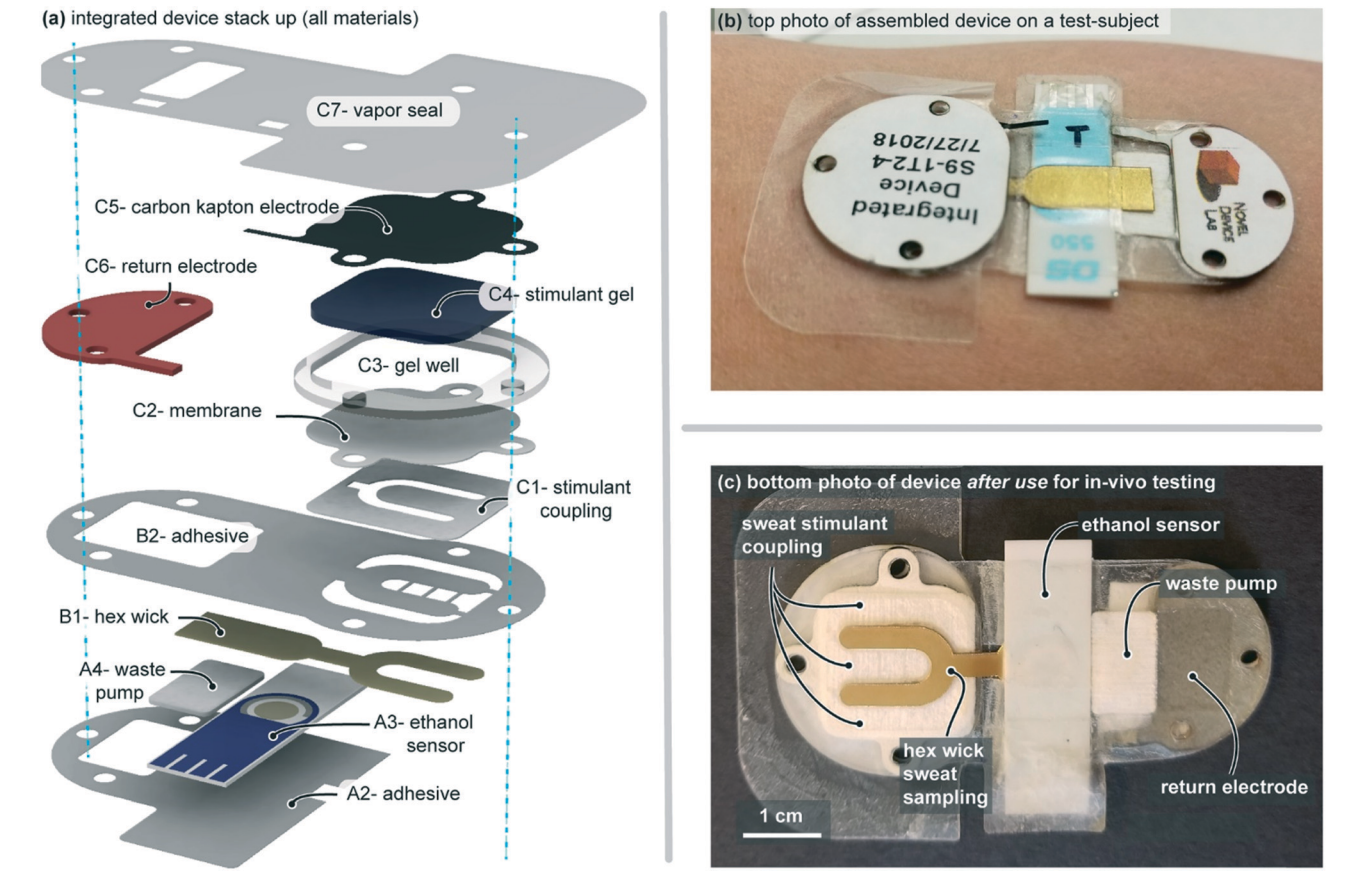

Fig. 1 Integrated device (a) system assembly and (b and c) photos of assembled devices. All ratios in (a) are to scale.

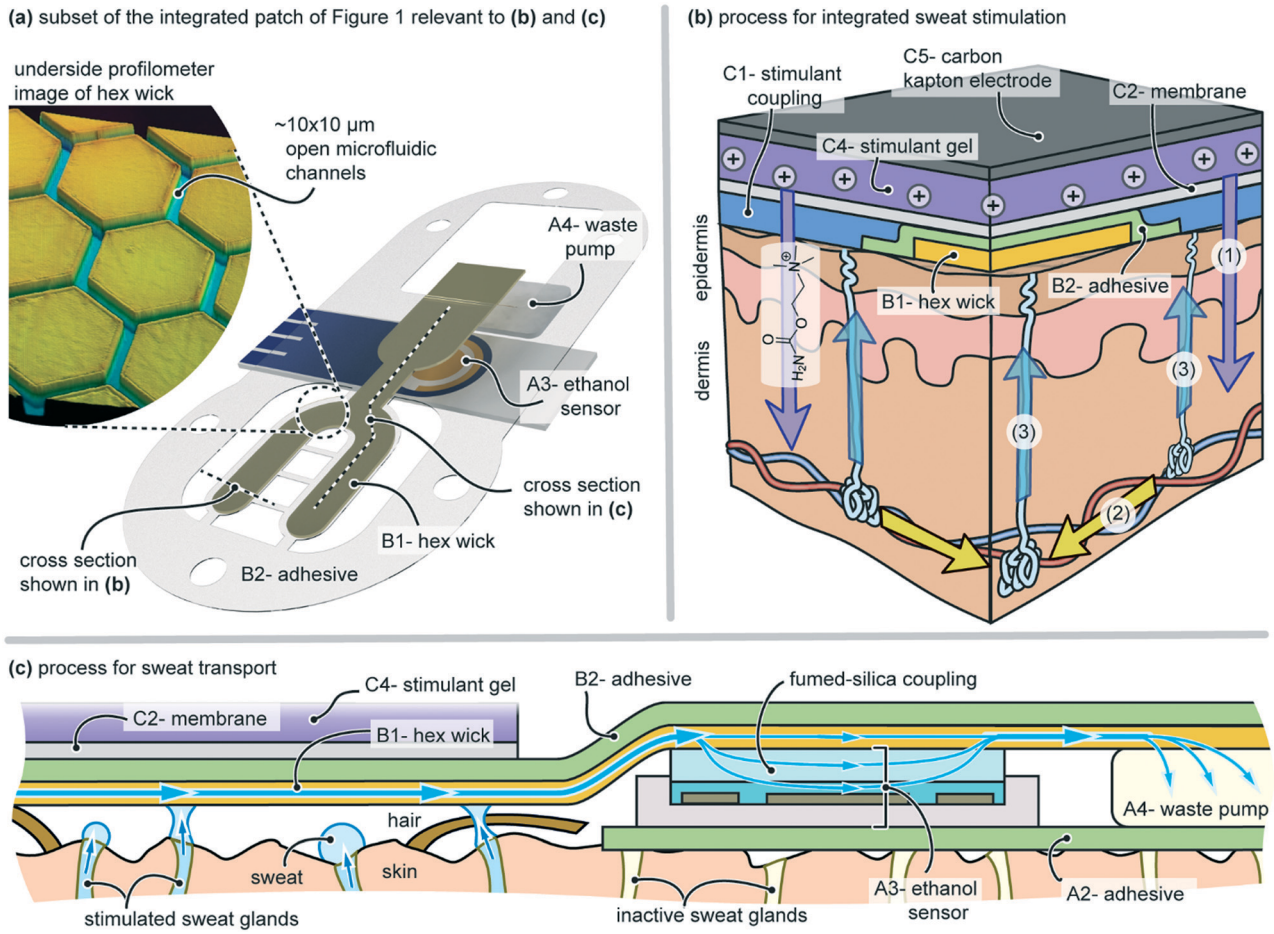

Fig. 2 Operational process of the integrated sweat-ethanol biosensing patch. Shown in (a) are a subset of components from Fig. 1 used to illustrate the device operation as described in (b) and (c). After the patch is applied (see Methods) (b) iontophoretic sweat stimulation involves (1) iontophoretic delivery of carbachol, (2) sudo-motor-axon cross-coupling of the stimulation response,[15] (3) stimulated sweat generation even in areas not directly underneath the stimulant gel. Because the dimensions are so small between the hex-wick and stimulation sites, cross-diffusional or direct iontophoretic stimulation is also possible.[15] After sweat is stimulated, the sweat is (c) wicked up from the skin by the hex-wick[16] and transported to the sensors and then onto the waste pump (see Methods). See Discussion section for a more detailed analysis of potential blood–sweat lag times regarding this wicking process.

Integrated sweat stimulation by iontophoresis involves three novel aspects. The first is membrane isolation (see Fig. 2b, C2) of the sweat stimulant from the skin, otherwise over time sweat will dilute out the stimulant and ions from sweat will iontophoretically dominate over the stimulant ions.[26] This was purely a design consideration we added in support of future work, as repeated sweat stimulation[27] was not performed in this paper. The second novelty is the use of carbachol as the stimulant, which provides a steady sweat generation rate for long durations (hours to days)[27] and, therefore, satisfies the steady sweat generation rate requirement noted in the introduction of this paper. The third is use of sudo-motor axon reflex sweating to help minimize mixing between the sweat stimulant materials (large volume of older contaminated sweat) and sweat that is swiftly transported to sensors (newer uncontaminated sweat).[15] This indirect stimulation process is shown and described in the diagram and caption for Fig. 2b.

Coupling sweat and sensors also involves several novel aspects. This generally uses an approach that we and others have increasingly employed compared to earlier reports of sweat biosensing: using microfluidics to transport sweat to sensors instead of placing the sensors directly on skin.[16,28–30] The first novelty is the use of the 'hex wick'[16] material that reduces the needed sample volume to ~100 nL cm^{-2} such that sweat is removed from the skin surface before significant skin-contamination could occur, and such that samples are quickly transported to the sensors to reduce lag time due to sampling fluidics. Sweat sampling and transport in the fully integrated system is best understood by discussing the two critical interfaces that the hex wick encounters (identified in Fig. 2c): the skin–wick interface and wick–sensor interface. The skin–wick interface reduces the volume and/or time of sweat wetting on the skin surface.[16] Once the skin–wick interface fills with sweat, bulk flow then moves swiftly to the sensor (~minutes, see Discussion section).

Another novelty is at the hex wick/sensor interface, where a film of fumed silica with gelatin binder is used to couple the hex wick and sensor surface. The fumed silica is a hydrophilic porous glass structure which readily absorbs water to ensure sweat completely wets the surface of the sensor, a requirement we had previously identified but not yet demonstrated (see Discussion section of Twine *et al.*[16]). Fumed-silica has distinct advantages over other fluid couplings (*e.g.*, rayon, paper, and hydrogels). It can be controllably deposited in very thin films to reduce sample volume requirements, it is shelf stable because when it dries the gelatin binder prevents cracking/shrinking and promotes rapid rewetting, and it can ensure the entire sensor surface remains wet in order to avoid interference of sensor signal due to changing wetting coverage (*i.e.*, variable sweat rate, body motion, *etc.*).[16]

Results

In vitro alcohol biosensor characterization results are shown in Fig. 3. The sensor employs an enzymatic electrode system which amperometrically measures concentrations of hydrogen peroxide that is created by metabolizing the ethanol with alcohol oxidase (*i.e.*, the sensor does not measure ethanol directly). A more detailed description can be found in the ESI.† Briefly, a linear concentration range is demonstrated over 0.014 to 3.67 mM with a correlation coefficient of 0.996 and 1.7 μM detection limit (Fig. 3a). This would correspond to ~0.02 BAC (measured as grams of ethanol per 100 mL of blood) and is a relatively low concentration range for physiologically relevant sweat ethanol but is adequate for the amount of alcohol consumed by human subjects in this proof of concept study.[17] A fully functional device capable of monitoring more extreme ethanol consumption would require a more robust sensor to be integrated. These sensors exhibited excellent repeatability with a 7.25 μA mM^{-1} cm^{-2} sensitivity and 3.95% relative standard deviation. Specificity testing showed minor responses to some of the interferents individually and when combined (Fig. 3b and c, respectively) in solution. However, the signal response to 1 mM ethanol (a relatively low sweat concentration) is significantly larger than this background interference. Furthermore, the interferent concentrations used here are much larger than the physiologically relevant interferent concentrations. It is important to note that this calibration of the sensors does not predict their behavior once fully integrated into the system and on-body. A loss in sensitivity is experienced when fluid is delivered to the sensor by a coupled hex wick. An uncoupled sensor submerged in sample (as in the calibration data) is purely diffusion limited where the coupled sensor suffers some from small but notable mass transport effects due to the miniscule sweat sample volumes delivered by the hex wick (*i.e.*, the coupled sensor does not sit within a relatively infinite source of analyte[16]). Additionally, the enzymatic sensors signal is affected by variations in sweat rate, salinity, pH, and temperature, and thus may vary based on a particular human subject's physiology and sweat conditions. This characterization

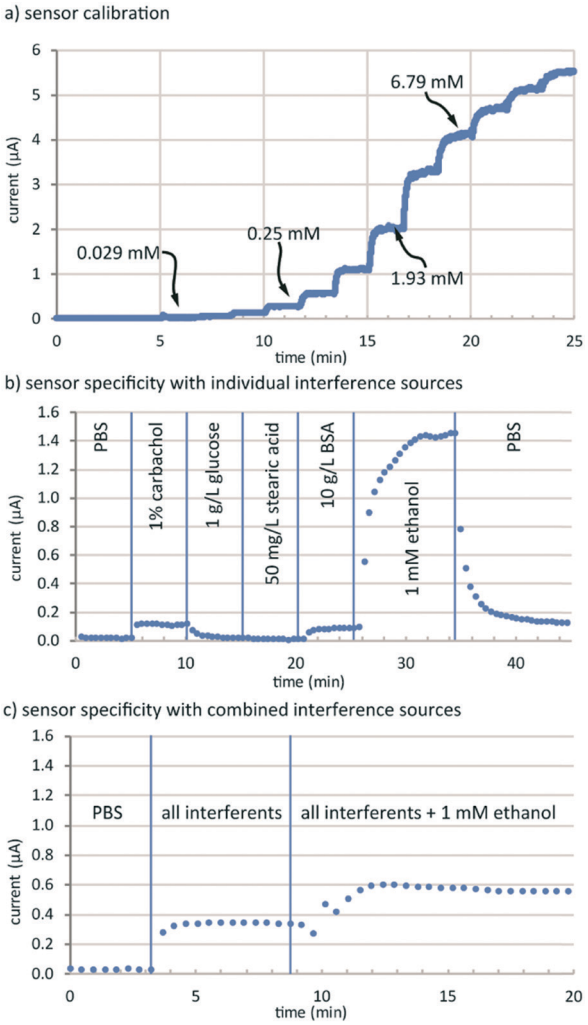

Fig. 3 Characterization data for the ethanol biosensor (a) ethanol response calibration, (b) specificity with individual interferent sources, (c) specificity with combined interferent sources. The concentrations of interferents tested are well above relevant physiological concentrations of the interferents.

is presented simply to demonstrate that the sensor behavior is specific to ethanol and that the sensor is not a significant source of error in the *in vivo* measurements.

In vivo results of two separate trials for each of two human subjects are depicted in Fig. 4. The plots provide the integrated sweat system's enzymatic ethanol sensor current (blue dots) and blood alcohol (BAC) measurements (red diamonds). Ethanol was chosen as the demonstration analyte because it is 1 : 1 in concentration between sweat and blood due to its small lipophilic nature.[2,13,17,18] Therefore, although sweat ethanol concentrations are not labelled on the left-hand axis of Fig. 4, the ethanol concentrations measured in sweat should match the BAC measured ethanol concentrations. Ethanol also allows a complete continuous measurement for >3 hours by (1) monitoring baseline condition followed by (2) a rapid blood and sweat rise and finally (3) physiological response of the body as it metabolizes and decreases the ethanol concentrations back to baseline.

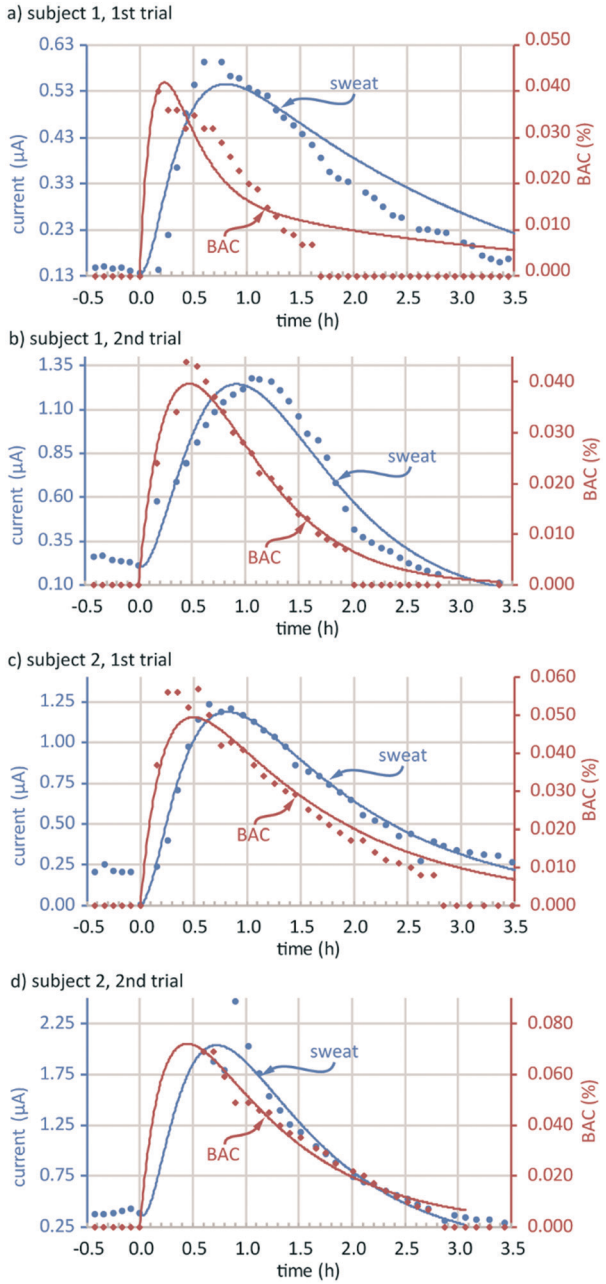

Fig. 4 *In vivo* test data and pharmacokinetic model curves fit to the data for (a and b) subject 1 trials 1 and 2, respectively, (c and d) subject 2 trials 1 and 2, respectively.

Data in Fig. 4 is presented such that the ethanol bolus occurs at time 0 h, and only 0.5 h of sensor results are shown previous to the ethanol bolus. The sweat ethanol sensor data has also been down sampled to match the BAC sampling interval (~5 min) for the purpose of modelling. Full data sets without down sampling (25 s), and collected over ~6 h, including sweat stimulation by iontophoresis, sensor settling, and steady state background sensor signal prior to bolus are provided in ESI† Fig. S1. These full data sets show ~1 h of data collected during active sweating but prior to bolus where a steady state background current is established (see Discussion). Importantly, this provides experimental control data for each *in vivo* trial, verifying the selectivity of the sensor and recording the non-zero background sensor current in sweat without ethanol.

The curve fits of Fig. 4 were obtained using the ordinary differential equations in eqn (1)–(3) that describe the three-compartment pharmacokinetic absorption and elimination model depicted in Fig. 5,

$$\frac{dA(t)}{dt} = -k_{abs} \times R_{ap} \times A(t) \quad (1)$$

$$\frac{dP(t)}{dt} = k_{abs} \times A(t) - (k_{PS1} + k_d) \times P(t) + C_{SP} \times S(t) \quad (2)$$

$$\frac{dS(t)}{dt} = -R_{SP} \times k_{SP2} \times S(t) + R_{SP} \times C_{PS} \times P(t) - k_d \times S(t) \quad (3)$$

where t is time, A is the concentration in the administration compartment, P is the concentration in the plasma, S is the sensor current, k_{abs} is absorption constant from the administration compartment to the plasma, k_{PS} and k_{SP} are absorption constants of ethanol exchange between the plasma and sweat, k_d is the elimination constant, and R_{AP} and R_{SP} are volume ratios of the administration compartment to the plasma compartment and sweat compartment to the plasma compartment respectively. To address current and concentration unit mismatches of the raw data, C_{SP} and C_{PS} are defined with the units of % μA^{-1} h^{-1} and μA $\%^{-1}$ h^{-1}, respectively. These represent products of conversion factor constants and differentiated ethanol exchange rate constants between sweat and plasma. Estimated values for these constants based on simulations are provided in ESI† Table S4.

Lag time is relevant to any health monitoring system that claims to be considered continuous and blood-correlated.[2]

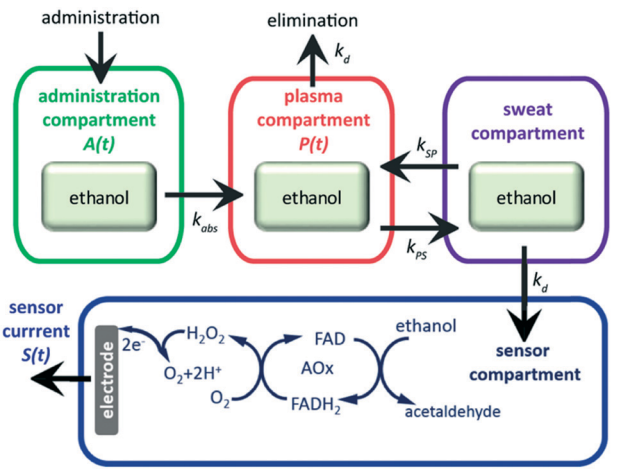

Fig. 5 Schematic depiction of the pharmacokinetic absorption and elimination model described by the eqn (1)–(3) and used for fitting curves to the *in vivo* data.

Table 1 provides lag times between bolus administration (*i.e.*, t = 0 h) and the time of initial sensor rise, the time to reach peak signal for the sensor and for the BAC, and the time to reach both of these events based on the modelling fits. The BAC measurement was limited by a 10–15 min minimum waiting period after bolus before the first sample could be collected, because residual alcohol in the mouth produces false elevated readings. Additionally, a 5 min minimum interval between BAC measurements was required to avoid saturating the BAC sensor with breath vapor and producing error messages. Thus, the initial response lag time for the breathalyzer was unable to be estimated. This also limited the curve fitting simulations for the sweat sensing system which instead was sampled every 25 s (see ESI† Fig. S1).

Discussion

We discuss here key interpretations of the data such as blood–sweat lag time and blood–sweat correlation. We will also discuss several limitations of the current device that should be the topic of future research and development.

Regarding lag times, the average time taken for the sweat ethanol signal to initially respond to ethanol was 6.5 min and as fast as 2.3 min. This was determined from when the sensor current continually exceeded one standard deviation above the mean of 10 min of background data measured prior to bolus (see ESI† Fig. S1 for full data sets). Lag time is certainly effected by sample volume and sweat generation rate (volume/(volume/min) = min) The continuous area of the hex wick material encompassing the skin and sensor area is ~1.55 cm^2 which for ~10 × 12 μm channels at 12% of the coverage area results in a ~220 nL contribution to total sample volume.[16] Additionally, the 20 μm thick fumed silica coupling over the 0.4 cm^2 sensor area with 45% liquid volume contributes 360 nL. This gives a ~600 nL total volume from skin to sensor. Sweat generation at the 0.8 cm^2 skin–wick interface provides 320 nL min^{-1} assuming 100 glands per cm^2 and 4 nL min^{-1} per gland. Thus, the time required for fresh sweat sample to completely exchange in the sample volume is 1.9 min. However, once at the sensor, analyte can also diffuse down to the active portion of the sensor and is not necessarily dominated by advective transport (mass-transport time), which could add to the total time lag. It is important to note, that the lag-times contributed by the large volume (mass-transport) and/or thickness (diffusion) of the sensor are not a fundamental limit, because in future work much smaller sensors could be custom-fabricated (~10's–100's μm diameter, <10 μm thick coupling).

Interestingly, although on average the sweat ethanol signal only lags the BAC by 6.5 min directly after bolus (assuming 0 min lag time for BAC), it lags by 6.9–35.13 min at the peak alcohol concentrations (10.5–32.2 min to peak BAC, 29.91–62.05 min to peak sweat sensor current). Although not previously reported for sweat, similar lag times have been observed in commercial skin vapor ethanol sensors.[31] This could suggest that partitioning of ethanol through body tissue may be more physiologically complex than has been previously concluded.[17,20,24,32] Prior sweat ethanol studies relied on limited data collection and employed methods where the sweat sample was allowed to mix over 20–30 min periods. For example, as can be seen by the quick rise of alcohol levels after bolus in Fig. 4, such prior reports would try to represent nearly the entire rise in ethanol concentration in a single sample, during which significant changes in concentration have occurred.

Regarding sweat ethanol and BAC correlation, although the results of Fig. 4 appear to correlate visually, we believe it is important to provide a numerical correlation method such that others can reproduce and test the results reported herein. With the exception of the data in Fig. 4a which showed an exponential relationship, the data for Fig. 4b–d all have a strong linear relationships for the decrease in ethanol concentration *vs.* time (model data: 0.9927, 0.9996, 0.9993, raw data: 0.9789, 0.9779, 0.9474). Regarding this correlation, there were two major factors that were considered. First, the data must be adjusted for lag time (see ESI† Table S5), which measurements of analyte concentrations and/or sweat flow rate. Here, for running correlations, we manually offset the data using lag times in Table 1, such that the sweat ethanol and BAC data overlap in time. Such methods are already used in practice for continuous glucose readers.[2] Secondly, we used a best tool presently available to us, which was to compare the decrease in sweat ethanol and BAC and assume a linear relationship *vs.* time. Sweat ethanol and BAC, in reality, will not exhibit linear time responses for bolus dosing, and more advanced correlation algorithms and software would likely be used in real-world application.

Table 1 Lag times from bolus administration (from t = 0)

Subject-trial ID	Initial sensor rise (min)	Sensor raw data peak (min)	BAC raw data peak (min)	Sensor model fit peak (min)	BAC model fit peak (min)
1–1	11.41	41.06	10.50	48.48	14.04
1–2	3.65	62.05	26.92	55.20	28.44
2–1	8.74	39.10	32.20	49.02	29.7
2–2	2.30	29.91	35.43[a]	43.50[a]	26.94[a]
Averages	6.53	43.03	23.21	49.05	24.78

[a] 1st ~35 min of BAC data after bolus was not recorded. Subsequently, sweat sensor data recorded over this period was not used for modelling. Not used for sweat sensor modelling as well. Not used for computing averages.

Although the correlation appears promising, there are several additional cautionary issues that should be raised. Firstly, the breathalyzer produces an algorithmic estimation of blood alcohol based on breath levels which could be a source of error since some studies question the absolute correlation of blood and breath alcohol.[33] A second potential issue is variable sweat rate (see Novel design and operation features section). Changing sweat rate changes the mass transport rate which is important because the ethanol sensor used here is also mass-transport-rate-limited (enzymatically consumes the ethanol).[15,34,35] We chose carbachol to mitigate this issue as much as possible in the present study due to its prolonged and steady rates,[27] and unlike previous studies[15,20,24,36] we wait 1 h before bolus dosing of ethanol to avoid the initial spike and decline in sweat rate for stimulated sweat.[27] However, we cannot guarantee that variable sweat generation rate is not a significant factor because we did not continuously measure sweat rate. We can draw some support from a previous study with two direct carbachol stimulations, subject 1 produced 2.8 to 1.4 nL min^{-1} per gland over 22.9 h, subject 3 produced 12.2 to 3 nL min^{-1} per gland over 24 h and subject 5 produced 2.3 to 1.5 nL min^{-1} per gland over 7 h.[27] During this study, we measured a sweat generation rate following the test for subject 2, 3 and 5 which were 1.33, 5.17, and 0.83 nL min^{-1} per gland (all measurements were taken after 5, 4.6, and 2 h respectively). This increases our confidence that variable sweat rate is not a major issue with the data presented here. Regardless, as noted in the introduction, we emphasize that most sweat biosensing devices will likely need to have integrated sweat rate sensors such that sensor signals can be trusted, and such that blood-to-sweat lag times can be continuously calculated and reported.[37] We also remind the reader that the non-ideal linear range of the enzymatic sensor is also a source of error. The ~0.07 maximum BAC level (measured as grams of ethanol per 100 mL of blood) measured in this study corresponds to ~15 mM of ethanol in blood. If sweat ethanol levels are truly 1 : 1 with blood, 15 mM is beyond the 3.67 mM upper bound to the linear range of the sensor. However, as explained in the Results, person-to-person sweat variations such as temperature, ionic strength and pH is likely much more significant source of error.

Regarding body motion effects, the quality of contact at the skin–wick and wick–sensor interfaces is also a critical consideration. For non-wicking, closed channel systems,[12,28–30] body movement can cause the sweat flow to accelerate or even reverse, which could cause false sensor readings. We employ the novel hex wick approach here not only for reducing sample volume and lag time,[16] but also for avoiding reversal of sweat flow in the device (uni-directional wicking flow to the waste pump[38]). A second issue with respect to body motion is interference with the sensor as caused by changing the wettability of the sensor, by disturbing any of the connecting leads of the sensor, and by damaging/altering the sensor itself with pressure or abrasion. Again, because our sensor is coated with chitosan and fumed silica, it is always fully wet. However, this does not prevent the other effects, any of which could have occurred in our data presented here. A most obvious example was when a subject needed to move considerably to use the restroom as seen in Fig. 4d at ~1 h (all such events are annotated in the ESI† raw data plots). Here, the sensor was disturbed so much that it needed to "resettle" over a 30 min period. The same behavior could be observed if the electrochemical sensor was electrically disconnected and then reconnected to the electrochemical analyzer (open-circuited, then close-circuited), reinforcing the speculation that the bulk of the noise was due to a poor electrical connection. Of course, future development work could resolve these purely-engineering challenges, but we raise them here to highlight the importance of obtaining raw sensor data with high temporal resolution.

As noted in the introduction, unresolved questions include the demonstration of such a device for 24 hours or greater, and with analytes that represent a greater breakthrough than those already commonly explored for sweat (electrolytes and metabolites). Regarding sweat stimulation, this work is incomplete if >24 operation is to be expected and serves only as a single usage event (hours) with a disposable platform. Moving toward days or even aspiring to a week or longer monitoring (such as in continuous glucose monitoring) will not be a trivial task. Beyond just the lack of data as proof, justification is provided in the Novel design and operation features section and in the ESI† materials (ESI Fig. S2 and S3 and supporting discussion) where our initial difficulties with integrated sweat stimulation are discussed. We believe that improved integrated sweat stimulation is the single-largest remaining *research* challenge for longer-term usage of the device, and our data or other's published data suggests that with further *development* work all other aspects of the device could achieve longer usage (days *etc.*).

Lastly, regarding sensors, in this work we used an enzymatic sensor technique that has been common for sweat biosensing demonstrations (ethanol, lactate, glucose). Other common techniques include ion-selective electrodes.[1] High value analytes such as hormones (cortisol, estrogen, testosterone, *etc.*) and proteins (cytokines, cardiac markers, *etc.*) have not yet been demonstrated with continuous blood-correlated data. Furthermore, we do not demonstrate a sensor here that is calibrated on body nor more desirably pre-calibrated in a reliable manner. Clearly, biosensor research is a significant need for not only sweat but also for other biofluid systems as well.[1,2,13]

Methods

Materials

A detailed bill of materials is provided in ESI† Table S2. Samples of materials 3M1577, 3M9793R and 3M1361 were obtained from 3M (Maplewood, MN). 99.9% agarose (A9539), alcohol oxidase (AOx) from *Pichia pastoris* (10–40 units per mg protein), chitosan, bovine serum albumin (BSA), glutaraldehyde, and sodium phosphate dibasic heptahydrate

($Na_2HPO_4{\cdot}7H_2O$) were obtained from Sigma-Aldrich (St. Louis, MO). Screen-printed electrodes (SPEs; DS550) made by DropSens (Llanera, Spain) were acquired from Metrohm (Riverview, FL). Tex Wipes, ethanol, potassium phosphate monobasic (KH_2PO_4), and sodium chloride were purchased from Fisher Scientific (Pittsburgh, PA). Ultrapure water (resistivity: 18.2 MΩ cm) was obtained from an EMD Millipore Direct-Q® 3 UV water purification system (Darmstadt, Germany). ITO PET (G430300) film was purchased from ShelDahl (Northfield, MN). SU-8 3000 was obtained from MicroChem (Westborough, MA). Carbachol 99% (CAS 51-83-2) was purchased from Professional Compounding Centers of America (PCCA, Houston, TX), NFX Nanofiltration membranes were obtained from Synder Filtration (Vacaville, CA). A carbon-coated Kapton film (<105 Ω per square, Kapton 200RS100) was purchased from Dupont (Wilmington, DE).

Fabrication and assembly

Sensors were fabricated in DropSens DS550 SPEs (Pt working, Pt counter and Ag pseudo reference electrodes). All reagents were used directly without further purification. All solutions were prepared using ultrapure water. A volume of 3 μL of an AOx–BSA composite (34.67 mg mL^{-1} AOx and 16.67 mg mL^{-1} BSA stabilizer) was drop cast onto the DS550 Pt working electrode which was then air dried for 30 minutes. This dried composite layer was then coated with a 3 μL droplet of a 1% weight chitosan solution in 1% acetic acid. This was then followed by a second 30 minute air drying. Crosslinking between the enzyme–BSA composite and chitosan was performed through the addition of a 2 μL volume of a 0.2% glutaraldehyde solution. This crosslinking reaction was allowed to proceed for 24 hours under ambient conditions. The fabricated sensors were then stored at 4 °C until further use.

Fumed silica was prepared by mixing 5% w/w fumed silica and 2.5% w/w gelatin in deionized (DI) water. Gelatin provides adhesion to the fumed silica and excellent abrasion resistance to the resultant dry film. Gelatin and fumed silica were stirred into the DI water at 80 °C until a homogeneous pasty mixture was achieved. After allowing to cool to 55 °C (safe temperature to apply to the AOx functionalized sensor), the paste was doctor bladed (Gardco 8″ Lokmicrom II) over the sensor area, defined by a laser cut contact adhesive mask (*i.e.*, over the working, reference and counter electrode area on the DropSens 550) and then allowed to air dry for ~10 min, resulting in ~20 μm thick dry fumed silica film.

The hex wick fabrication protocol followed Twine *et al.*[16] Briefly, bulk sheets of the 10 μm wide × 12 μm deep hexagonal channel array were patterned with SU-8 on 250 μm thick PET film by photolithography. Hex wicks were then laser cut (Universal Laser VLS3.50) from those bulk sheets to the custom footprint for the integrated system. They were cleaned by rinsing with isopropanol and deionized water and then by oxygen plasma (Plasmatic Systems Plasma Preen II). Sputter deposition (Denton Desk II) of 60 nm of gold was performed and then immediately followed by thiol functionalization with 3-mercapto-1-propanesulfonate (MPS) or a custom triple thiol (7-mer)[16] by soaking for 12 min in solution.

Carbachol gel discs were fabricated using 1% carbachol and 3% agarose, by weight, in deionized water. The carbachol and agar solution was first heated to 150 °C and stirred for 30 minutes. The aqueous solution of carbachol remains stable even when heated.[39] Next, deionized water lost due to evaporation during the heating/stirring process was added back to the solution and this solution was then again heated at 80 °C for 30 minutes to ensure the added water was evenly distributed. The carbachol/agarose solution was then cast in an acrylic mold which provided an array of discs. The mold was then placed into a refrigerator at 8 °C where the discs were allowed to solidify. Finally, the carbachol discs were removed from the mold and stored at 8 °C in a plastic bag containing 1% carbachol in deionized water.

An AutoCAD file of the assembly layers, a schedule detailing the function and preparation of each layer (Table S3†), and a time lapse video of assembly are provided in the ESI.† Referencing Fig. 1a, layers A1–A3 were assembled in ascending order on the alignment tool. Next, the hex wick (layer B1) was aligned and placed on adhesive layer B2 by hand (*i.e.*, without the alignment tool). Assembly B was then placed onto assembly A on the alignment tool (good alignment results in the fumed silica coated sensor area being completely covered by the expansion in the hex wick at the wick–sensor interface, see Fig. 1b and 2a). Then, layers C1–C7 were placed in ascending order on the A & B assembly using the alignment tool (note: upper adhesive layers B2 and C7 are slightly wider than others to allow conformation to the changing device profile as it is built and thus require working over vertical surfaces for a clean finish, see AutoCAD file in ESI†). Finally, test identifiers were adhered to the patch (Fig. 1b).

Sensor characterization

The electrochemical characterization of the fabricated biosensor(s) was carried out by using a Reference 600 electrochemical workstation from Gamry Instruments (Warminster, PA). To obtain the chronoamperometric response, the electrode interface of the sensor was immersed in 0.1 M phosphate buffered saline (PBS) at a pH of 7.2. Using a potential of +0.6 V, the amperometric response was recorded for 100 seconds at each alcohol concentration. There was a total of 13 alcohol concentrations used which covered a range of 0.014–9.51 mM. This characterization was performed in triplicate (n = 3).

In vivo testing

Human under the guidance of the University of Cincinnati's subjects testing was performed (UC) Human Research Protection Program (ID# 2016-4769 approved by the UC Institutional Review Board).

The volar surface of the subject's dominate forearm was cleaned with isopropanol and deionized water to remove

potential contaminants. Then, the adjoining contact material of the membrane isolation stimulation assembly was wetted with 1% carbachol in DI water immediately before placing the patch on the cleaned area and initiating the monitoring of the sensor. Iontophoresis (0.28 mA cm^{-2}, 42 mC cm^{-2}, corresponding to a 3 min dosing event) was performed utilizing a commercial iontophoresis unit (ActivaDose II, ActivaTek, Gilroy, CA). These levels of iontophoresis have been utilized previously and are equivalent to the commercially available Wescor Nanoduct system.[15,26,27] Sweat was allowed to completely wet the sensor (monitored as the rise of significant current measurements by the sensor, typically within 10 min after stimulation) and the sensor allowed to settle to a stable background current (~60 minutes after fully wet). The subject was then given ~80 mL of 40% alcohol (80 proof) mixed into ~240 mL of a soft drink. BAC was measured three times before the subject consumed alcohol, then every ~5 minutes afterward by a breathalyzer (BACTrack S80). The sweat ethanol sensor current was monitored for the rise and fall of signal (*i.e.*, absorption and elimination of ethanol, ~3–4 hours).

The fully assembled integrated patch was connected to a PalmSens4 electrochemical analyzer using a standard Palmsens sensor cable modified by cutting off the factory ends and soldering them onto a breakout board. A flat flexible cable (FFC) connected the sensor electrodes to the breakout board using *z*-axis tape at the sensor and an FFC connector soldered onto the breakout board. A repeating chronoamperometry method was used to monitor sensors with an electrochemical analyzer and software (PalmSens4 and PSTrace 5.4 software). A potential of 0.6 V *vs.* Ag pseudo-reference was applied to the sensor for 10 s, and then the cell was turned off for 15 s before repeating. The 10 s data point for each chronoamperogram was used for the measurement.

Statistical analysis

The ordinary differential equation based model was implemented in the Python programming language, which is available at (www.python.org). The differential equations were simulated using the *ODEint* solver that is implemented within the SciPy package. To estimate the parameters for each subject, a differential evolution algorithm (*optimize.differential_evolution* that is available within the SciPy package) was used to minimize the mean sum of squared error between the model simulation and the experimental data. For consistency, and to reduce the chance of overfitting to the sensor measurements, only sensor measurements with a corresponding BAC measurement were used as inputs for parameter fitting. The time of alcohol administration was used as the initial time point, and the initial conditions for the BAC and sensor were set with their experimental levels at this time point. The initial condition for the absorptive compartment, which was not measured experimentally, was assumed to be 5 (a.u.) for all subjects.

For data correlation, as detailed in the Discussion section, the data sets were adjusted for lag times and only the decreasing ethanol concentrations correlated assuming a linear fit. Fits are represented by R^2 values and include a 95% confidence interval. The 95% confidence interval for R^2 is calculated based on a bootstrap method where the original data was sampled 500 times with replacement and the R^2 value calculated for each resampled data. The variation among these R^2 values are the basis for the confidence interval estimation. Finally, for all linear fits, the simple Pearson correlation can be found by taking the square root of R^2.

Conflicts of interest

Corresponding author Jason Heikenfeld has an equity interest in Eccrine Systems, Inc., a company that may potentially benefit from the research results, and also serves on the company's Board. The terms of this arrangement have been reviewed and approved by the University of Cincinnati in accordance with its conflict of interest policies.

Acknowledgements

The authors would like to acknowledge support from the Air Force Research Labs Award #USAF contract # FA8650-15-C-6625, NSF EPDT Award #1608275, and the Ohio Federal Research Network (PO FY16-049; WSARC-1077-700). We also acknowledge the industrial members of the Center for Advanced Design and Manufacturing of Integrated Microfluidics (NSF I/UCRC award number IIP-1738617). This research was supported in part by an appointment to the Student Research Participation Program at the U.S. Air Force Research Laboratory, 711th Human Performance Wing, Human Effectiveness Directorate, Human-Centered Intelligence, Surveillance and Reconnaissance Division administered by the Oak Ridge Institute for Science and Education through an interagency agreement between the U.S. Department of Energy and USAFRL. The authors would also like to thank Mekibib Altaye and Gabriel Lyon from the Cincinnati Children's Hospital Medical Center for their support in analyzing and correlating data.

References

1 J. Heikenfeld, A. Jajack, J. Rogers, P. Gutruf, L. Tian, T. Pan, R. Li, M. Khine, J. Kim, J. Wang and J. Kim, *Lab Chip*, 2018, **18**, 217–248.
2 J. Heikenfeld, A. Jajack, B. Feldman, S. W. Granger, S. Gaitonde, G. Begtrup and B. A. Katchman, *Nat. Biotechnol.*, 2019, in press.
3 W. Gao, S. Emaminejad, H. Y. Y. Nyein, S. Challa, K. Chen, A. Peck, H. M. Fahad, H. Ota, H. Shiraki, D. Kiriya, D. H. Lien, G. A. Brooks, R. W. Davis and A. Javey, *Nature*, 2016, **529**, 509–514.
4 H. Lee, T. K. Choi, Y. B. Lee, H. R. Cho, R. Ghaffari, L. Wang, H. J. Choi, T. D. Chung, N. Lu, T. Hyeon, S. H. Choi and D. H. Kim, *Nat. Nanotechnol.*, 2016, **11**, 566–572.

5 W. Jia, A. J. Bandodkar, G. Valdés-Ramírez, J. R. Windmiller, Z. Yang, J. Ramírez, G. Chan and J. Wang, *Anal. Chem.*, 2013, **85**, 6553–6560.
6 A. J. Bandodkar, D. Molinnus, O. Mirza, T. Guinovart, J. R. Windmiller, G. Valdés-Ramírez, F. J. Andrade, M. J. Schöning and J. Wang, *Biosens. Bioelectron.*, 2014, **54**, 603–609.
7 S. Imani, A. J. Bandodkar, A. M. V. Mohan, R. Kumar, S. Yu, J. Wang and P. P. Mercier, *Nat. Commun.*, 2016, **7**, 11650.
8 D. P. Rose, M. E. Ratterman, D. K. Griffin, L. Hou, N. Kelley-Loughnane, R. R. Naik, J. A. Hagen, I. Papautsky and J. C. Heikenfeld, *IEEE Trans. Biomed. Eng.*, 2015, **62**, 1457–1465.
9 D. Morris, S. Coyle, Y. Wu, K. T. Lau, G. Wallace and D. Diamond, *Sens. Actuators, B*, 2009, **139**, 231–236.
10 X. Huang, Y. Liu, K. Chen, W. J. Shin, C. J. Lu, G. W. Kong, D. Patnaik, S. H. Lee, J. F. Cortes and J. A. Rogers, *Small*, 2014, **10**, 3083–3090.
11 B. Schazmann, D. Morris, C. Slater, S. Beirne, C. Fay, R. Reuveny, N. Moyna and D. Diamond, *Anal. Methods*, 2010, **2**, 342.
12 A. Koh, D. Kang, Y. Xue, S. Lee, R. M. Pielak, J. Kim, T. Hwang, S. Min, A. Banks, P. Bastien, M. C. Manco, L. Wang, K. R. Ammann, K. I. Jang, P. Won, S. Han, R. Ghaffari, U. Paik, M. J. Slepian, G. Balooch, Y. Huang and J. A. Rogers, *Sci. Transl. Med.*, 2016, **8**, 366ra165.
13 J. Heikenfeld, *Electroanalysis*, 2016, **28**, 1242–1249.
14 W. Ament, J. Huizenga, G. Mook, C. Gips and C. J. Verkerke, *Int. J. Sports Med.*, 1997, **18**, 35–39.
15 Z. Sonner, E. Wilder, T. Gaillard, G. Kasting and J. Heikenfeld, *Lab Chip*, 2017, **17**, 2550–2560.
16 N. B. Twine, R. M. Norton, M. C. Brothers, A. Hauke, E. F. Gomez and J. Heikenfeld, *Lab Chip*, 2018, **18**, 2816–2825.
17 M. J. Buono, *Exp. Physiol.*, 1999, **84**, 401–404.
18 Z. Sonner, E. Wilder, J. Heikenfeld, G. Kasting, F. Beyette, D. Swaile, F. Sherman, J. Joyce, J. Hagen, N. Kelley-Loughnane and R. Naik, *Biomicrofluidics*, 2015, **9**, 031301.
19 M. Gamella, S. Campuzano, J. Manso, G. G. de Rivera, F. López-Colino, A. J. Reviejo and J. M. Pingarrón, *Anal. Chim. Acta*, 2014, **806**, 1–7.
20 J. Kim, I. Jeerapan, S. Imani, T. N. Cho, A. Bandodkar, S. Cinti, P. P. Mercier and J. Wang, *ACS Sens.*, 2016, **1**, 1011–1019.
21 H. Lee, C. Song, Y. S. Hong, M. S. Kim, H. R. Cho, T. Kang, K. Shin, S. H. Choi, T. Hyeon and D. Kim, *Sci. Adv.*, 2017, **3**, e1601314.
22 S. Y. Oh, S. Y. Hong, Y. R. Jeong, J. Yun, H. Park, S. W. Jin, G. Lee, J. H. Oh, H. Lee, S. S. Lee and J. S. Ha, *ACS Appl. Mater. Interfaces*, 2018, **10**, 13729–13740.
23 L. C. Tai, W. Gao, M. Chao, M. Bariya, Q. P. Ngo, Z. Shahpar, H. Y. Y. Nyein, H. Park, J. Sun, Y. Jung, E. Wu, H. M. Fahad, D. H. Lien, H. Ota, G. Cho and A. Javey, *Adv. Mater.*, 2018, **1707442**, 1707442.
24 J. Kim, J. R. Sempionatto, S. Imani, M. C. Hartel, A. Barfidokht, G. Tang, A. S. Campbell, P. P. Mercier and J. Wang, *Adv. Sci.*, 2018, 1800880.
25 A. Hauke, L. S. S. Kumar, M. Y. Kim, J. Pegan, M. Khine, H. Li, K. W. Plaxco and J. Heikenfeld, *Biosens. Bioelectron.*, 2017, **94**, 438–442.
26 P. Simmers, Y. Yuan, Z. Sonner and J. Heikenfeld, *Biomicrofluidics*, 2018, **12**, 034101.
27 P. Simmers, S. K. Li, G. Kasting and J. Heikenfeld, *J. Dermatol. Sci.*, 2018, **89**, 40–51.
28 A. Martín, J. Kim, J. F. Kurniawan, J. R. Sempionatto, J. R. Moreto, G. Tang, A. S. Campbell, A. Shin, M. Y. Lee, X. Liu and J. Wang, *ACS Sens.*, 2017, **2**, 1860–1868.
29 H. Y. Y. Nyein, L. Tai, Q. P. Ngo, M. Chao, G. B. Zhang, W. Gao, M. Bariya, J. Bullock, H. Kim, H. M. Fahad and A. Javey, *ACS Sens.*, 2018, **3**, 944–952.
30 J. R. Sempionatto, A. Martin, L. García-Carmona, A. Barfidokht, J. F. Kurniawan, J. R. Moreto, G. Tang, A. Shin, X. Liu, A. Escarpa and J. Wang, *Electroanalysis*, 2018, 1–8.
31 T. E. Karns-Wright, J. D. Roache, N. Hill-Kapturczak, Y. Liang, J. Mullen and D. M. Dougherty, *Alcohol Alcohol.*, 2017, **52**, 35–41.
32 T. Kamei, T. Tsuda, Y. Mibu, S. Kitagawa, H. Wada, K. Naitoh and K. Nakashima, *Anal. Chim. Acta*, 1998, **365**, 259–266.
33 J. Vukovic, D. Modun and D. Markovic, *J. Subst. Abus. Alcohol*, 2015, **3**, 1–5.
34 H. Zhu, L. Li, W. Zhou, Z. Shao and X. Chen, *J. Mater. Chem. B*, 2016, **4**, 7333–7349.
35 A. Sonawane, P. Manickam and S. Bhansali, *IEEE Rev. Biomed. Eng.*, 2017, **10**, 174–186.
36 S. Emaminejad, W. Gao, E. Wu, Z. A. Davies, H. Yin Yin Nyein, S. Challa, S. P. Ryan, H. M. Fahad, K. Chen, Z. Shahpar, S. Talebi, C. Milla, A. Javey and R. W. Davis, *Proc. Natl. Acad. Sci. U. S. A.*, 2017, 201701740.
37 J. Heikenfeld, USA Patent Application, US20150112165A1, 2015.
38 A. Alizadeh, A. Burns, R. Lenigk, R. Gettings, J. Ashe, A. Porter, M. McCaul, R. Barrett, D. Diamond, P. White, P. Skeath and M. Tomczak, *Lab Chip*, 2018, **18**, 2632–2641.
39 *The Merck Index: An Encyclopedia of Chemicals, Drugs, and Biologicals*, ed. M. J. O'Neil, Royal Society of Chemistry, Cambridge, UK, 15th edn, April 2013, p. 1607, ISBN 9781849736701.